cancers

MDPI

Article

Endogenously-activated ultrasmall-in-nano therapeutics: assessment on 3D head and neck squamous cell carcinomas

Melissa Santi [1*], Ana Katrina Mapanao,[1,2] Domenico Cassano,[1] Ylea Vlamidis,[1] Valentina Cappello,[1] and Valerio Voliani[1*]

[1] Center for Nanotechnology Innovation@NEST, Istituto Italiano di Tecnologia, Piazza San Silvestro, 12-56126, Pisa, Italy.

[2] NEST-Scuola Normale Superiore, Piazza San Silvestro, 12-56126, Pisa, Italy.

* Correspondence: melissa.santi@iit.it; valerio.voliani@iit.it

Received: date; Accepted: date; Published: date

Abstract: Negative or positive HPV-associated Head and Neck Squamous Cell Carcinomas (HNSCCs) are high recurrence neoplasms usually resulting in a poor prognosis, mainly due to metastasis formation. Despite the low overall patients survival rate and the severe side effects, the treatment of choice is still cisplatin-based chemotherapy. Here, we report a straightforward protocol for the production of high throughput 3D models of negative or positive HPV-associated HNSCCs, together with their employment in the therapeutic evaluation of gold ultrasmall-in-nano architectures comprising an endogenously-activatable cisplatin prodrug. Beyond enhancing the biosafety of cisplatin, our approach paves the way for the establishment of synergistic co-therapies for HNSCCs based on excretable noble metals.

Keywords cancer; cisplatin; 3D models; nanomaterials; theranostics.

1. Introduction

Head and Neck squamous cell carcinoma (HNSCC) is a complex group of malignancies that affect different body sites, among which oral cavity, nasopharynx, oropharynx, larynx, and salivary glands. HNSCC is one of the most common cancer types with 53.000 new cases estimated in 2019 only in the United States,[1] and it is mainly caused by extensive consumption of tobacco and alcohol.[2] Usually, HNSCCs are characterized by mutation of p53 and p16 genes and often result in a poor prognosis and high risk of recurrence/metastasis (R/M HNSCC).[3] Recently, a new subset of HNSCC with peculiar biological and clinical features was associated to Human Papilloma Virus (HPV) infection.[4,5] HPV-16 and HPV-18 subtypes have the highest incidence and induce malignancies both in HNSCC and cervical cancers.[6] They encode for E6 and E7 viral proteins, which induce dysregulation of the cell cycle interacting with p53 and pRb respectively.[7] HPV-positive cancer patients usually show better survival rates respect to HPV-negative counterparts with an improved overall survival, but the molecular mechanisms of these responses are still debated.[8,9] When possible, patients are primarily subjected to local surgery and radiotherapy, followed by chemotherapy which instead is the only treatment in the case of R/M HNSCC.[10] Single or combined cisplatin-based therapies are the principal treatments for HNSCCs neoplasms and their sensitivity is similar for ±HPV-associated conditions, even if their sub-optimal efficacy is limited by associated severe systemic toxicities, such as nephrotoxicity, neurotoxicity, ototoxicity, and emesis.[11] In this context, Pt(IV) complexes provide an attractive alternative to Pt(II) compounds because of their inertness results in fewer side effects, decreased drug inactivation and longer half-life in the bloodstream.[12] Pt(IV) prodrugs are hidden forms of cisplatin, whose production is triggered by

endogenous thiols, such as glutathione, which lead to reductive elimination of axial ligands.[13] The inclusion of Pt(IV) prodrugs in biodegradable nanomaterials enhances the specificity of cisplatin due to the defined localization and endogenously-double-controlled release of the active drug.[14] Beyond drug delivery, the conjugation of prodrugs with nanomaterials, and in particular to noble metals, is essential for the development of innovative or combined/enhanced treatments.[15,16] For example, nanostructured noble metals can be exploited for their peculiar behaviors also in photothermal therapy,[17] radiation therapy enhancement,[18] and in imaging applications as ultrasound or photoacoustic.[19,20] On the other hand, despite the massive efforts, co-treatments based on noble metal nanomaterials are still at preclinical stage, due to the body persistence issue.[16,21] Hitherward, our group has introduced biodegradable/excretable nano-architecture (NAs) composed by silica nanocapsules comprising plasmonic ultrasmall noble metal nanoparticles, that may bring again inorganic nanomaterials to the forefront of clinical applications.[21,22] Indeed, NAs jointly combine the behaviors of plasmonic nanomaterials with a good clearance rate of the building blocks.[23,24] Besides demonstrating their massive production and protocol reproducibility,[15,25] we have already confirmed their biosafety,[24,26] assessed the biokinetics,[23,24] and currently identified some potential applications.[14,17,19,20] Here, NAs comprising a Pt(IV) prodrug (NAs-cisPt) were produced and the therapeutic efficacy fully assessed on customized 3D models of two ±HPV-associated HNSCCs cell lines: SCC-25 (HPV-negative) and UPCI:SCC-154 (HPV-positive). 3D models better represent the neoplasms complexity with respect to 2D cell cultures and result useful for the progress of preclinical oncological investigations and the translation of nanomaterials to clinics.[27,28] Different type of 3D models are available and can be used depending on the types of research that have to be carried out: cells can be induced to form tridimensional structures or can be embedded in specific scaffold that mimic extracellular matrix (e.g Matrigel).[29,30] Some models can also present more complex structures, like Corio-allontoic membranes (CAMs), for pharmacological studies that include also the vascular component.[31] Among all, tumor spheroids represent the best option for the study of nanoparticles efficacy, since they are composed by different populations of quiescent/necrotic and proliferative cells, comprising gradients of nutrients and oxygen and at the same time are cheap and easily to handle.[32] Indeed, 3D tumor models are composed by different populations of quiescent/necrotic and proliferative cells, comprising gradients of nutrients and oxygen.[33] In particular, they allow to obtain reliable information on nanomaterials efficiency and internalization mechanisms, taking also into account cell–cell and cell–extracellular matrix (ECM) interactions.[34]·[35] Overall, our findings are a significant step forward to the translation of novel and efficient noble metal-based co-treatments to patients.

2. Results and Discussion

In this work, we have employed NAs internally-labelled with Alexa Fluor-647 (NAs-647) or internally-loaded with a cisplatin prodrug (NAs-cisPt) to investigate, respectively, the internalization behaviors and the cytotoxicity trends in 2D and 3D SCC-25 and UPCI:SCC-154. NAs-cisPt were synthesized following the protocol employed for the production of standard passionfruit-like nanoarchitectures (NAs) with slight modifications, as described in our previous works (Figure 1A).[14,19] Briefly, ultrasmall gold nanoparticles (USNPs) were synthesized by fast reduction of an aqueous solution of chloroauric acid by sodium borohydride in the presence of poly(sodium 4-styrene sulfonate) (PSS). Then USNPs were mixed with a Pt(IV) prodrug-modified poly-L-lysine aqueous solution in order to form controlled aggregates. Finally, the polymer templates were employed to compose a 20-nm-thick silica shell by using a modified Stöber process.[22] Resulting NAs-cisPt contain 4.9% and 1.4% (w/w) of, respectively, gold and platinum (meaning 21 μg/mg of cisPt/nano-architectures) on the total freeze-dried sample weight, quantified by Inductively Coupled Plasma Mass Spectrometry (ICP-MS) analysis. A full set of characterizations was performed to check the products and the reproducibility of the protocol **(Figure S1 and Table S1)**. Standard NAs (silica capsule comprising only USNPs) and Alexa Fluor 647-modified NAs (NAs-647) were produced and

routine characterized as reported elsewhere.[14,23] The general structure of all nano-architectures is reported in **Figure 1A** and **Figure S2**. NAs-647 were firstly employed in order to evaluate by confocal microscopy their internalization behaviors in ±HPV-associated HNSCCs. The nano-architectures were efficiently internalized in SCC-25 and UPCI:SCC-154 cell lines by endocytosis, as confirmed by the characteristic punctate signals arising from nanoparticles inside endocytic vesicles and lysosomes **(Figure S3)**. This result was not surprising, as both bare and labelled NAs have generally demonstrated good internalization behaviors also in 2D cell cultures and 3D of MIA PaCa-2, a model of pancreatic ductal adenocarcinoma (PDAC).[14,35] It is worth to remember that the internalization features of the three versions of nano-architectures (NAs, NAs-cisPt, and NAs-647) are expected to be similar because there are no differences in their external surfaces, as supported as well by comparable zeta potential surface charge (**Table S1**). Indeed, also NAs-cisPt were efficiently internalized in both ±HPV-associated HNSCCs, inducing cell death with a differential sensitivity **(Figure 1C)**. Surprisingly, UPCI-SCC-154 resulted slightly more sensitive to cisplatin with respect to SCC-25, and this finding is also consistent with the IC_{50} values calculated by WST-8 viability assay (8.2±0.1 μM and 3.5±0.1 μM, respectively for -HPV and +HPV HNSCC) associated to the effect of the drug alone **(Figure 1B and Table S2)**. Indeed, several works have discussed that ±HPV-associated HNSCCs have not a different sensitivity to cisPt rather than radiotherapy.[36] It is worth to notice that NAs-cisPt produced significant effects on cell lines **(Figure 1C)** only after 48h from incubation. This behavior is related to the degradation timeframe of the nano-architectures (24 hours) followed by the conversion of the prodrug to its active form, that is able to penetrate the nucleus and binds the DNA, inducing the therapeutic action.[14]

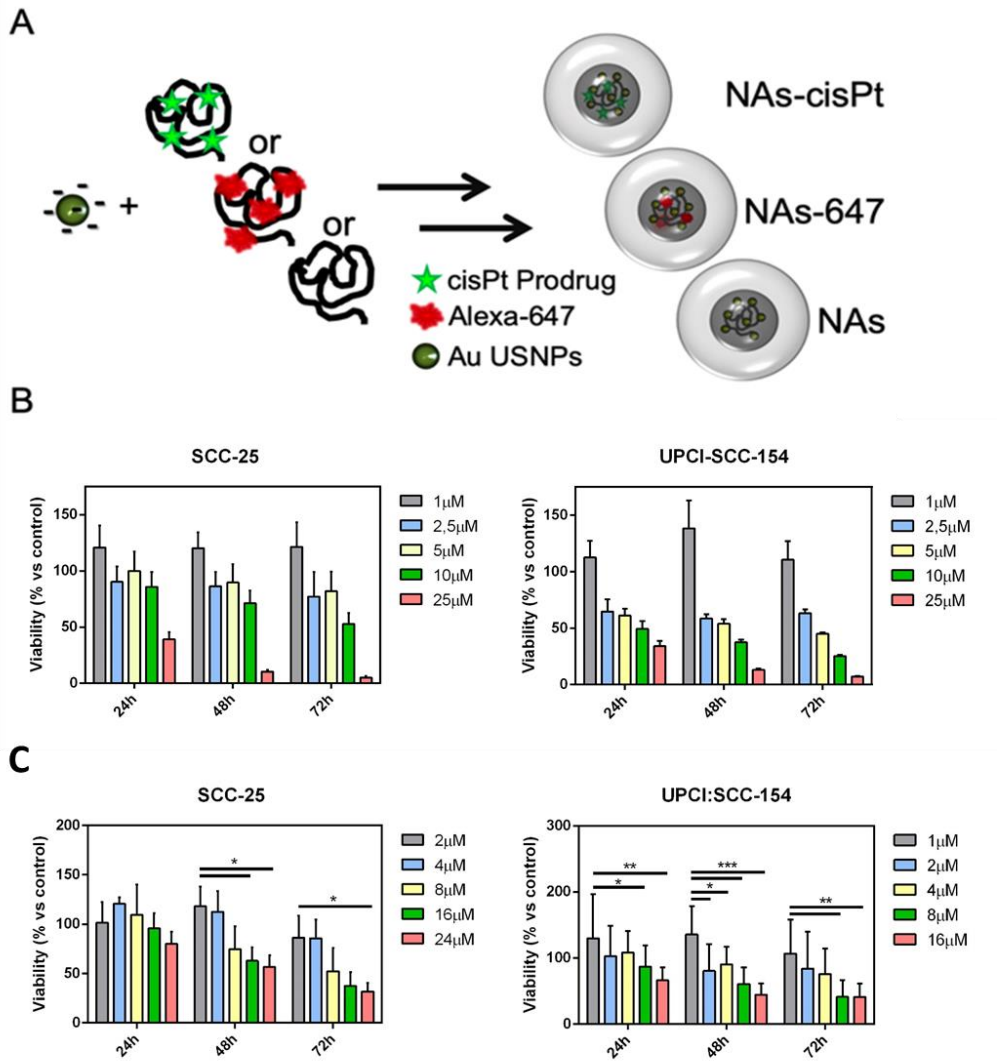

Figure 1. Structures of NAs and cytotoxic effect of cisplatin-loaded NAs against SCC-25 and UPCI-SCC-154. (A) Cartoon depicting the production protocol of the 3 kind of NAs employed in this work. Each cell line was treated with increasing concentrations of (B) free cisplatin or (C) NAs-cisPt, for 2 hours at 37°C and 5% of CO_2. Cells viability was measured at 24h, 48h and 72h after treatment, and data were normalized to the viability of control cells (treated only with medium). Concentrations in the graph correspond to the active cisplatin comprised in NAs-cisPt. Results are the average of three independent experiments and error bars state the standard deviation. Two-way ANOVA Dunnett's test for (B) vs. 1 μM, *p≤ 0,05 and for (C) vs. 2 μM or 1 μM for SCC-25 and UPCI:SCC-154 respectively, *p<0.05.

Additional viability assays with standard NAs were performed to confirm that the observed cytotoxic effect of NAs-cisPt was effectively induced by released cisplatin. The amount of nano-architectures employed to treat cells was normalized on gold, *i.e.* the amount of gold (and thus of nano-architectures) employed was similar for each condition with both NAs and NAs-cisPt (**Figure S4**). As already demonstrated on zebrafish and murine models, the biosafety of standard NAs was also confirmed for these cell lines.[23,24,26]

Multicellular tumor spheroids (MCTSs) are high-throughput and accessible models that well-represent neoplasms.[35] They possess more complex biological features compared to monolayer cell cultures and allow the investigation of important features such as cell-cell and cell-extracellular matrix interactions. These behaviors play a fundamental role on the effective therapeutic action of nanostructured materials. Furthermore, although investigations on animal models remain inevitably

important in preclinical studies, more strict directives are now being implemented (such as the European Directive 2010/63/EU) to encourage the use of alternative biological systems in order to promote a more responsible employment of animals in research (3R's concept: reduce, refine, and replace).[37] 3D models of ±HPV-associated HNSCCs were produced by a slightly modified protocol of the hanging drops approach from Foty et al.[38] A cell suspension containing $1x10^6$ cells/mL was used to produce drops on the lid of a petri dish. A volume of 10 µl or 20 µl was used, respectively for SCC-25 and UPCI-SCC-154, to prepare drops. After 3 days, a sheet of cells is formed in each drop that was transferred to a suspension plate in order to induce cell aggregation by orbital shaking (**Figure S6**). The spheroids produced by our standardized protocol show a diameter of 200-400 µm for both cell lines, and their structure was evaluated by transmission electron microscopy (**Figure S5**).

Firstly, with the ultrastructural analysis we were able to confirm the presence of the virus in UPCI:SCC-154 cell cytoplasm **(Figure S7A)**. Both cell monolayers showed a high number of microvilli that were able also to form tight junctions in the corresponding three-dimensional structures. More specifically, SCC-25 form compact structures with an external layer of dividing cells and an internal layer with necrotic cells. Here, the presence of junctions was more pronounced as evidenced by the inset in **Figure S5C**. On the other hand, UPCI-SCC-154 formed less compact spheroids that show an internal empty cavity. In particular, cells were arranged in different layers like a sandwich. Four different layers were identified from TEM analysis: starting from the periphery the first two layers are formed by viable cells, followed by one internal necrotic portion and a final layer composed again of living cells, as also demonstrated from the poor staining of the third layer in **Figure S7B**. Interestingly, a very dense matrix surrounds cells of both 3D models.

The complex three-dimensional structure of the spheroids, highlighted by the ultrastructural analysis, strongly supports reliable investigations of the effects of novel nanomaterials on ±HPV-associated HNSCCs. Spheroids of both ±HPV-associated HNSCCs were treated with NAs-647 for 2h and the nanoparticles internalization process was followed for 72h by confocal microscopy (**Figure 2**). Immediately after incubation and for the first 24h, the nano-architectures showed the typical punctate pattern due to endocytic internalization. It is worth to notice that despite the surrounding matrix and the complexity of the system, the nano-architectures were efficiently internalized in both the models. Indeed, as demonstrated by the ultrastructural analysis spheroids usually present different layers of cells as a consequence of gradients of oxygen and nutrients; among all, only the external layer is composed by actively dividing cells, thus the ability of our nanostructures to reach the first cell layer and to have a cytotoxic effect is a significant result. Furthermore, the fluorescence signal was spread inside cells after 48h, confirming the degradation of the silica shell and the release of the dye in the cytosol. Finally we would like to underline that confocal microscopy is a good technique that allow to obtain preliminary results about qualitative nanoparticles distribution in cells. Unfortunately, the major limit of this optical method is related to the single focal plane imaging. A more quantitative analysis on precise nanoparticles internalization was reported later in this work.

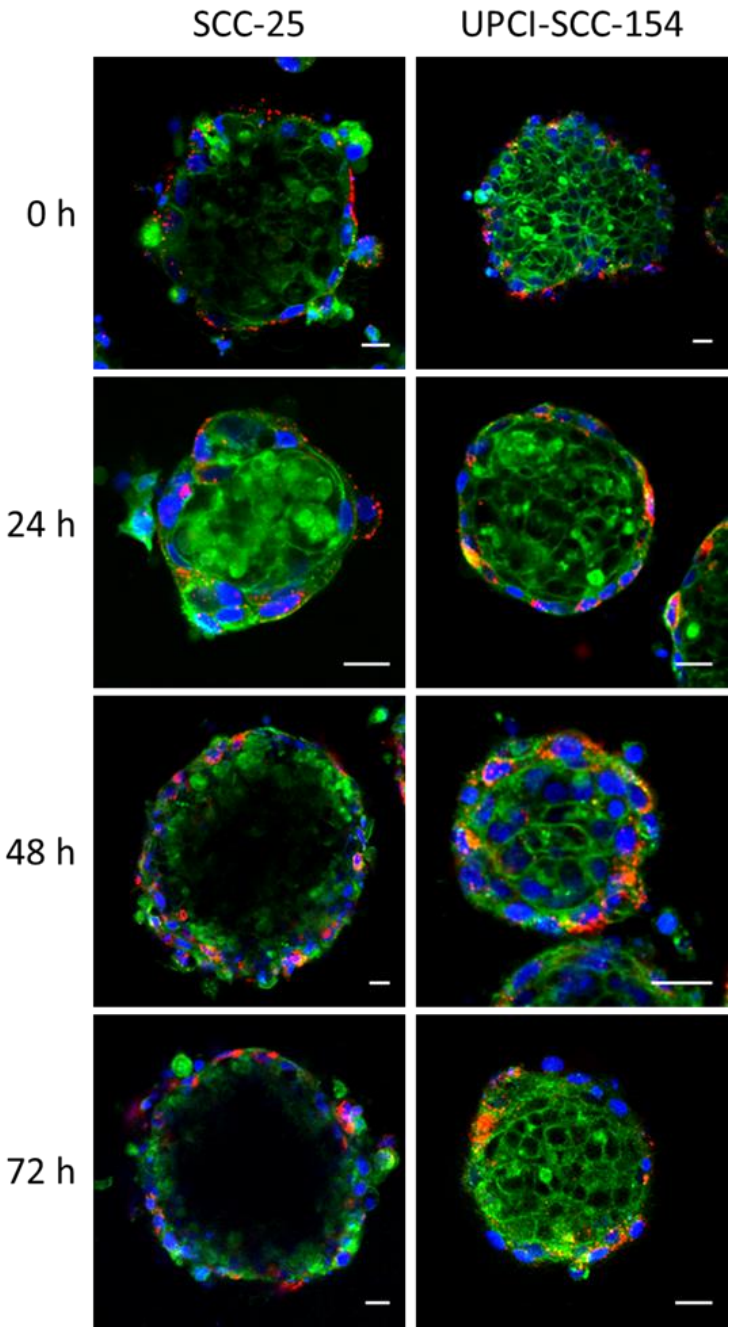

Figure 2. Confocal analysis of nanoparticles internalization in 3D models of HNSCC cell lines. SCC-25 and UPCI-SCC-154 spheroids were incubated with fluorescently labeled nanoparticles (NAs-647). A cell membrane marker (CellMask Green-488, Life Technologies) and Hoechst 33342 (Sigma) for nuclei were used. Spheroids were washed twice with PBS and imaged by confocal microscopy. Scale bar: 100 μm.

Finally, spheroids of the two cell lines were treated with increasing concentration of NAs-cisPt (corresponding to increasing concentration of cisplatin) for 2h, in order to evaluate their therapeutic effect. The viability was calculated using the CellTiter-Glo® 3D Cell Viability Assay, until 72h after treatment (**Figure 3**). We preferred to use a commercial test because other approach like size changes were useless with these two cell lines. Indeed, we saw that in general, the spheroids obtained from SCC-25 and UPCI:SCC-154 cell lines do not change in size once formed. This is probably due to the presence of the extracellular matrix layer, that we confirmed by TEM analysis. On this regard, we have also observed that these spheroids cannot be used for more than two weeks because cells

continue to divide until they reach a saturation level (in which they start to die) without the spheroids demonstrate substantial change in size.

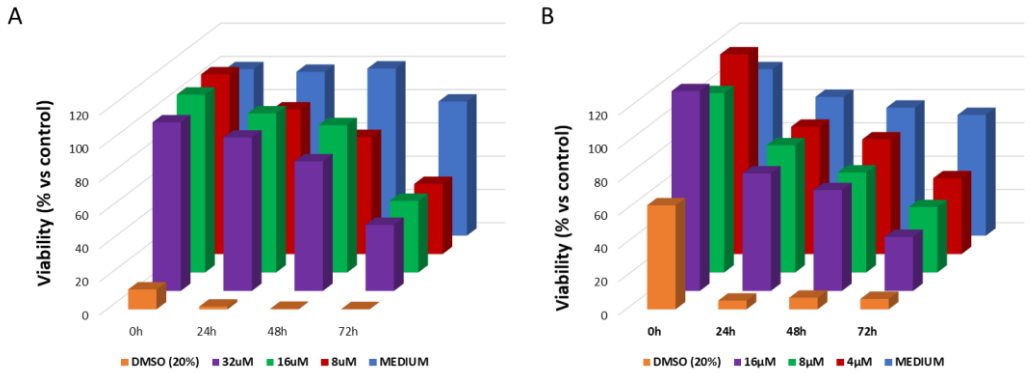

Figure 3. Cytotoxic effect of cisplatin-loaded nanoparticles on 3D models of HNSCCs. Cells of (A) SCC-25 and (B) UPCI-SCC-154 were treated with increasing concentration of NAs-CisPt. Spheroids without any treatments (MEDIUM) and treated with a solution of Dimethyl Sulfoxide 20% v/v (DMSO) were used respectively as negative and positive controls. Cytotoxicity was monitored from 0h to 72h using the CellTiter-Glo® 3D Cell Viability Assay. Results are the average of three independent experiments (error bars are resumed in **Table S2 and S3**). Two-way ANOVA Dunnett's test vs. MEDIUM, no significant statistical differences were found.

In general, NAs-cisPt affected the spheroids viability for both cell lines, confirming the distribution of the nano-architectures in the 3D models. Interestingly, viability of SCC-25 is almost constant for all the tested concentrations. This trend is probably associated with a plateau in the internalization rate of the nano-architectures. On the other hand, UPCI-SCC-154 demonstrated a dose-dependent viability trend, and this behavior may be associated to both the different density of cells in the spheroids and the cellular adhesion. As for 2D cultured cells, a slightly increased sensitivity of UPCI-SCC-154 to cisplatin respect to SCC-25 was observed. In order to confirm that this effect is not associated to a different endocytosis rate in 3D models, the gold content inside spheroids was quantified by ICP-MS after 2h incubation with the same amount of NAs-cisPt. As expected, the amount of gold was almost similar in both samples (0.29 ± 0.0013 and 0.27 ± 0.012 µg/µg gold/lysate, respectively for UPCI-SCC-154 and SCC-25). Thus, the effect may be associated to a potential different release trend of the drug in the cell lines. These results suggest that NAs-cisPt are efficiently internalized in these 3D cell culture models and induce an effective cell death with a reduced off-target action resulted by the double-controlled endogenous release. It is also worth to notice that, due to the presence of plasmonic USNPs, NAs are promising nanoplatforms for combined therapies and for theranostics development.

3. Materials and Methods

All chemicals were purchased from Sigma-Aldrich unless otherwise specified. All chemicals were used as received.

3.1. Synthesis of standard nano-architectures

Synthesis of gold nanoparticles. Ultrasmall gold nanoparticles with a diameter of approximately 3 nm were prepared according to the following procedure. To 20 mL of milliQ water, 10 µL of poly(sodium 4-styrene sulfonate) (70 kDa, 30% aqueous solution, PSS) and 200 µL of $HAuCl_4$ aqueous solution (10 mg/mL) were added. During vigorous stirring, 200 µL of sodium borohydride (8 mg/mL in milliQ water) was added quickly, and the mixture was vigorously stirred for 2 minutes. After the addition of $NaBH_4$, the solution underwent some color changes until becoming a brilliant orange. Before its use, the solution was aged for 10 minutes and employed without further purification.

Synthesis of gold nanoparticle arrays w/o dyes. 20 mL of gold nanoparticle solution was added to a 50 mL round bottomed flask followed by 200 μL water solution of poly(L-lysine) hydrobromide 15–30 kDa (PL, 20 mg/mL or the same amount of a dye-modified poly-Lysine), and the mixture was allowed to stir for 20 minutes at room temperature. The as-synthesized gold aggregates were collected by centrifugation (13400 rpm for 3 minutes), suspended in 2 mL of milliQ water and sonicated for a maximum of 4 minutes.

Synthesis of Dye-Modified Poly(L-Lysine)–PLa. Poly(L-lysine) hydrobromide 15–30 kDa (1.5 mg) was dissolved in PBS (780 μL) and AlexaFluor 647-NHS ester (200 μg, Invitrogen) was added to the solution. The reaction mixture was kept under stirring overnight at RT, and it was used without further purification.

Synthesis of nano-architectures (NAs). 70 mL of absolute ethanol followed by 2.4 mL of ammonium hydroxide solution (30% in water), and 40 μL of tetraethyl orthosilicate (TEOS, 98%) were added in two 50 mL plastic Falcon tubes. Then 2 mL of the gold nanoparticle arrays previously prepared were added to the Falcon (1 mL each) and the solution was allowed to gently shake for a further 3 h. The as-synthesized NAs were collected by 30 minutes centrifugation at 4000 rpm, washed twice with ethanol to remove unreacted precursors and suspended in 1 mL of ethanol. A short spin centrifugation was employed in order to separate the structures over 150 nm from the supernatant, which was recovered as a pink-iridescent solution. The solution containing about 1.5 mg of NAs was stored at -20°C until use. It remains usually stable for at least 1 year. Product recovery: (i) 2 minutes centrifugation at 13 400 rpm, (ii) remove the colorless supernatant, and (iii) add the solvent of interest. The solubility of NAs in water, buffers, and physiological fluids is tested for up to 60 mg/mL.

3.2. Synthesis of drug loaded nano-architectures

Synthesis of c,t,c-[$PtCl_2(OH)_2(NH3)_2$]. The method used was based on the one previously described by Hall et al.[39] Cis-[$PtCl_2(NH_3)_2$] (0.40 g, 1.33 mmol) was suspended in milliQ water (10 mL) and H_2O_2 30% (w/v) (14 mL, tenfold excess) was added. The mixture was stirred for 1 h at 50 °C. Then it was cooled to 0 °C and saturated water solution of NaCl (10 mL) was added. The resulted pale yellow powder was collected by filtration and washed with cold water, ethanol and diethyl ether, and dried in a vacuum pump, yielding c,t,c-[$PtCl_2(OH)_2(NH_3)_2$] (223 mg, 0.67 mmol, 50%).

Synthesis of c,t,c-[$PtCl_2(NH_3)_2(OH)(O_2CCH_2CH_2CO_2H)$]. The method used was based on that previously described by Dhar et al.[12] To a solution of c,t,c-[$PtCl_2(OH)_2(NH_3)_2$] (0.2 g, 0.6 mmol) in anhydrous dimethyl sulfoxide (DMSO, 16 mL) was added succinic anhydride (0.06 g, 0.6 mmol) and the reaction mixture was stirred at room temperature for 12 h. The solution was freeze-dried and acetone (10 mL) was added to precipitate a light yellow solid, which was collected by filtration and washed several times with acetone, diethyl ether, and then dried in a vacuum pump, yielding c,t,c-[$PtCl_2(NH_3)_2(OH)(O_2CCH_2CH_2CO_2H)$] (0.16 g, 0.37 mmol, 62%). 1H NMR (DMSO-d6) 6.18–5.66 (m, 6H), 2.44–2.33 (m, 4H). 13C NMR (DMSO-d6) 31.16; 31.74; 174.55; 180.17.

Synthesis of Drug-Modified Poly(L-Lysine)–PLp. c,t,c-[$PtCl_2(NH_3)_2(OH)(O_2CCH_2CH_2CO_2H)$] (0.5 mg) was dissolved in PBS buffer (400 μL) and mixed with of freshly made EDC/NHS (40 μL, 0.21 M) milliQ water solution (EDC: N-(3-dimethylaminopropyl)-N′-ethylcarbodiimide hydrochloride, NHS: N-Hydroxysuccinimide). After 10 min stirring at room temperature, poly(L-lysine) hydrobromide 15–30 kDa (75 μL, 20 mg/mL milliQ solution) was added to the reaction mixture and the resulting solution was stirred overnight at room temperature. The modified poly(L-lysine) was collected and washed three times with PBS buffer by Amicon 10 K filter units, and then dissolved in PBS buffer (800 μL).

Synthesis of cisplatin loaded nano-architectures (NAs-cisPt). The protocol used is the same as that of standard nanoparticles but in this case we used drug-modified poly(L-lysine) to form gold nanoparticles arrays.

3.3. Dynamic Light Scattering (DLS) measurements

Measurements by DLS were performed at 37 °C in a 1 mL polypropylene cuvette on a Zetasizer nano-ZS DLS (Malvern Instruments) following the manufacturer's instructions. PBS solutions of nanomaterials were analyzed with a single scattering angle of 90°. Each value reported is the average of five consecutive measurements.

3.4. Inductively Coupled Plasma Mass Spectrometry (ICP-MS) Analysis

The amount of gold and platinum inside nanoparticles were measured by ICP-MS analysis. 10µl of samples was digested in 200 µl of aqua regia at 80-100 °C for 4 hours. Then the solution was diluted to 2 mL and analyzed by ICP-MS (7700 series ICP-MS, Agilent Technologies). To measure the amount of gold in spheroids, each sample was firstly lysate with 100 µl of RIPA buffer for 1h and the protein content was measured by Bradford assay. Then samples were digested with 200 µl of aqua regia at 80-100 °C and diluted to 2 mL for ICP-MS analysis. The gold content was expressed as µg of gold/µg of lysate.

3.5. UV–Vis Spectrophotometry

The absorption spectra were obtained using a double-beam Jasco V-550 spectrophotometer. The samples in PBS (1×) were placed in quartz cuvettes with a 1.5 mm path length.

3.6. Transmission Electron Microscopy

The TEM observations of particles and cells were performed in ZEISS Libra 120 PLUS operating at 120 KV and equipped with an In-column Omega filter. The colloidal solutions of the nanoparticles (5 µL) were deposited to a 300-mesh of carbon coated copper grids.

3.7. Ultrastructure Analysis of 2D and 3D cultures of SCC-25 and UPCI-SCC-154

2D cell culture or spheroids in suspension have been fixed in 1,5% glutaraldehyde in sodium cacodylate buffer (0.1 M pH 7.4) for 1 h at room temperature and then treated for resin embedding. Briefly, scraped cells or recovered spheroids were kept in a new fixative solution (overnight at 4 °C), then the samples were postfixed 1 h (1% OsO_4 plus 1% $K_3Fe(CN)_6$ sodium cacodylate buffer; 0.1 M pH 7.4), and stained with 3% solution of uranyl acetate in 20% ethanol. Finally, they were dehydrated in a growing series of ethanol gradient and embedded in epoxy resin (Epon 812, Electron Microscopy Science, Hatfield, PA, USA). Polymerization has been performed for 48 h at 60 °C. In order to perform ultrastructural analysis, 90 nm sections of the treated samples were cut by using UC7 (Leica Microsystems, Vienna, Austria) and collected on 300 mesh copper grids (EMS).

3.8. Cell culture

Human squamous cell carcinoma SCC-25 and UPCI-SCC-154 were purchased from the American Type Culture Collection (ATCC). SCC-25 were maintained in a complete growth medium composed by a 1:1 mixture of Dulbecco's modified Eagle's medium and Ham's F12 medium while UPCI-SCC-154 were growth in Dulbecco's modified Eagle medium (DMEM) from Invitrogen (Carlsbad, CA). Both growth mediums were supplemented with 10% fetal bovine serum (FBS), 4mM L-glutamine, 1 mM sodium pyruvate, 100 U/mL penicillin, and 100 mg/mL streptomycin (Invitrogen). SCC-25 medium was also supplemented with 400 ng/mL of hydrocortisone. Cells were maintained at 37 °C in a humidified 5% CO2 atmosphere. For 3D structures, we used a modified protocol from Foty et al.[38] Briefly, cells were harvested and centrifuged for 5 min at 1200 rpm and then resuspended in fresh medium, counted and the suspension was adjusted to a final concentration of 1 x 10^6 cells/mL. Afterwards, 10 µL (for SCC-25) or 20 µL (for UPCI-SCC-154) of cells were placed on the lid of a 100 mm cell culture dish that was flipped into the chamber containing 10 mL of PBS. Cells were left to settle into the drops until they form a sheet and then were transferred to a 100 mm suspension culture dish after 3 days. Finally, cell aggregates were placed inside a CO_2 incubator with an orbital shaker (70 rpm) for 24h to induce the formation of the proper spherical shape.

3.9. Confocal Microscopy

Cells were seeded 24 h before the experiments into glass-bottom Petri dish (WillCo-dish GWSt-3522) to reach 80%–90% of confluence. Incubation of nanoparticles (maximum 30 μg) was performed for 30 min at 37 °C, 5% CO2 in complete medium (DMEM) with 10% FBS (total volume of 1 mL). After incubation cells were washed twice with PBS, fresh medium was added and the samples were analyzed by confocal microscopy. For experiments with 3D models, 3-4 spheroids for each experimental condition were imaged using 2D and 3D samples were imaged on an Olympus FV1000 inverted confocal laser scanning microscope equipped with a thermostat chamber set at 37°C and 5% CO_2. The lasers for excitation were 405, 488 and 633 nm. All images were analyzed using Fiji-ImageJ software version 1.51 s.

3.10. Viability Assay on 2D cell culture

The cytotoxicity of cisplatin, NAs and NAs-cisPt was evaluated by using a tetrazolium salt, 2-(2-methoxy-4-nitrophenyl)-3-(4-nitrophenyl)-5-(2,4-disulfophenyl)-2H tetrazolium, and monosodium salt (WST-8) assay. SCC-25 and UPCI-SCC-154 cells (1×10^4 cells per well) were seeded in 96 well plates. After being cultured for 24 h, the cells were incubated with a 2% serum-containing medium in the presence of free drug or nanoparticles at increasing concentration in medium (100uL) for 30 min at 37 °C. After incubation, the medium was removed and cells were washed twice with PBS and kept in fresh medium. For each experimental time point cells were incubated with WST-8 reagent (100 μL) and 2% serum-containing medium (90 μL) for 2 h. Absorbance (450 nm) was measured using a microplate reader (Glomax Discovery, Promega). The percentage of cell viability was determined by comparing drug-treated cells with the untreated cells (100% viability). Data represent the average of three independent experiments. Error bars represent the SD from three independent experiments.

3.11. Viability Assay on 3D cell models

Viability of 3D spheroids was evaluated using the CellTiter-Glo® 3D Cell Viability Assay (Promega, Milan, Italy). Treated or untreated spheroids for each time point were transferred separately from a round-bottom 96-well plate to a white 96-well plate for luminescence measurements with 100 μL of medium. Then 100 μL of CellTiter-Glo® 3D reagent was added to each well, the plate was shaken for 5 minutes and the luminescence signal was recorded after 25 minutes of incubation with a microplate reader (Glomax Discovery, Promega). Cell viability was determined respect to the viability of spheroids maintained in complete medium without any other treatments.

4. Conclusions

In summary, we have described a robust protocol for the production of fully-characterized 3D ±HPV-associated HNSCCs models together with their employment in nanomaterials efficacy evaluation. Biodegradable and excretable NAs comprising cisPt prodrug can be efficiently internalized in 2D and 3D cell culture and have demonstrated an endogenously-double-controlled therapeutic activity, showing interesting toxicity trends. . In particular, we evidence more than 50% decrease of cell viability of our 3D models in both cell lines in 72 h after treatment.Moreover, the exploitation of the Pt(IV) complexes can limit the systemic toxicity of cisplatin paving the way for more efficient management of HNSCCs. Remarkably, excretable gold USNPs comprised in NAs-cisPt also enable the potential integration of noble metal-driven imaging and treatments, supporting the development of safe co-treatments for HNSCCs.

Supplementary Materials: The following are available online at www.mdpi.com/xxx/s1, Fig. S1: Physical-chemical characterization of NAs-CisPt, Fig. S2: General structure of nano-architectures, Fig. S3: Internalization of NAs-647 in HNSCC-25 and UPCI-SCC-154 cell lines, Fig. S4: Cytotoxic effect of Cisplatin against HNSCC-25 and UPCI-SCC-154, Fig. S5: Cytotoxic effect of standard gold nanoparticles against SCC-25 and UPCI-SCC-154, Fig. S6: Bright field images of SCC-25 and UPCI-SCC-154 spheroids, Fig. S7: Ultrastructural characterization of

different layers of 3D UPCI-SCC-154, Table S1: Size and zeta potential of NAs, NAs-647 and NAs-cisPt, Table S2: IC50 measurements for SCC-25 and UPCI-SCC-154 measured 24h after treatment with free or nanoparticles-loaded cisplatin, Table S3: Viability of SCC-25 spheroids after treatment with NAs-cisPt, Table S4: Viability of UPCI-SCC-154 spheroids after treatment with NAs-cisPt.

Author Contributions: D.C., A.K.M., Y.V. and M.S. performed nano-architectures synthesis and characterizations; M.S. and A.K.M. designed and performed biological experiments; V.C. and M.S. performed the EM experiments; V.V. designed the project and co-projected the biological experiments. All Authors have discussed the data and contributed to write the manuscript.

Supporting Information: The following files are available free of charge. Supporting Materials (file type, PDF).

Acknowledgments: The research leading to these results has received funding from AIRC under MFAG 2017 – ID 19852 project – P.I. Voliani Valerio.

Conflicts of Interest: The authors declare no competing financial interest.

References

1. Siegel, R.L.; Miller, K.D.; Jemal, A. Cancer statistics, 2019. *CA. Cancer J. Clin.* **2019**, *69*, 7–34.
2. Lewin, F.; Norell, S.E.; Johansson, H.; Gustavsson, P.; Wennerberg, J.; Birklund, A.; Rutqvist, L.E. Smoking tobacco, oral snuff, and alcohol in the etiology of squamous cell carcinoma of the head and neck. *Cancer* **1998**, *82*, 1367–1375.
3. Ho, A.S.; Kraus, D.H.; Ganly, I.; Lee, N.Y.; Shah, J.P.; Morris, L.G.T. Decision making in the management of recurrent head and neck cancer. *Head Neck* **2014**, *36*, 144–151.
4. Wang, L.; Zhang, P.; Molkentine, D.P.; Chen, C.; Molkentine, J.M.; Piao, H.; Raju, U.; Zhang, J.; Valdecanas, D.R.; Tailor, R.C.; et al. TRIP12 as a mediator of human papillomavirus/p16-related radiation enhancement effects. *Oncogene* **2017**, *36*, 820–828.
5. Mirghani, H.; Amen, F.; Tao, Y.; Deutsch, E.; Levy, A. Increased radiosensitivity of HPV-positive head and neck cancers: Molecular basis and therapeutic perspectives. *Cancer Treat. Rev.* **2015**, *41*, 844–852.
6. Guo, T.; Califano, J.A. Molecular Biology and Immunology of Head and Neck Cancer. *Surg. Oncol. Clin. N. Am.* **2015**, *24*, 397–407.
7. Bose, P.; Brockton, N.T.; Dort, J.C. Head and neck cancer: From anatomy to biology. *Int. J. Cancer* **2013**, *133*, 2013–2023.
8. Koneva, L.A.; Zhang, Y.; Virani, S.; Hall, P.B.; McHugh, J.B.; Chepeha, D.B.; Wolf, G.T.; Carey, T.E.; Rozek, L.S.; Sartor, M.A. HPV Integration in HNSCC Correlates with Survival Outcomes, Immune Response Signatures, and Candidate Drivers. *Mol. Cancer Res.* **2018**, *16*, 90–102.
9. Coordes, A.; Lenz, K.; Qian, X.; Lenarz, M.; Kaufmann, A.M.; Albers, A.E. Meta-analysis of survival in patients with HNSCC discriminates risk depending on combined HPV and p16 status. *Eur. Arch. Oto-Rhino-Laryngology* **2016**, *273*, 2157–2169.
10. Dok, R.; Nuyts, S. HPV positive head and neck cancers: Molecular pathogenesis and evolving treatment strategies. *Cancers (Basel).* **2016**, *8*.
11. Sacco, A.G.; Cohen, E.E. Current treatment options for recurrent or metastatic head and neck squamous cell carcinoma. *J. Clin. Oncol.* **2015**, *33*, 3305–3315.
12. Dhar, S.; Daniel, W.L.; Giljohann, D.A.; Mirkin, C.A.; Lippard, S.J. Polyvalent Oligonucleotide Gold Nanoparticle Conjugates as Delivery Vehicles for Platinum(IV) Warheads. *J. Am. Chem. Soc.* **2009**, *131*, 14652–14653.
13. Wang, X.; Guo, Z. Targeting and delivery of platinum-based anticancer drugs. *Chem. Soc. Rev.* **2013**, *42*, 202–224.
14. Cassano, D.; Santi, M.; Cappello, V.; Luin, S.; Signore, G.; Voliani, V. Biodegradable Passion Fruit-Like Nano-Architectures as Carriers for Cisplatin Prodrug. *Part. Part. Syst. Charact.* **2016**, *33*, 818–824.
15. Cassano, D.; David, J.; Luin, S.; Voliani, V. Passion fruit-like nano-architectures: a general synthesis route. *Sci. Rep.* **2017**, *7*, 43795.
16. Cassano, D.; Pocoví-Martínez, S.; Voliani, V. Ultrasmall-in-Nano Approach: Enabling the Translation of Metal Nanomaterials to Clinics. *Bioconjug. Chem.* **2018**, *29*, 4–16.
17. Cassano, D.; Santi, M.; D'Autilia, F.; Mapanao, A.K.; Luin, S.; Voliani, V. Photothermal effect by NIR-responsive excretable ultrasmall-in-nano architectures. *Mater. Horizons* **2019**, *6*, 531–537.
18. Daraee, H.; Eatemadi, A.; Abbasi, E.; Fekri Aval, S.; Kouhi, M.; Akbarzadeh, A. Application of gold nanoparticles in biomedical and drug delivery. *Artif. Cells, Nanomedicine, Biotechnol.* **2016**, *44*, 410–422.
19. Avigo, C.; Cassano, D.; Kusmic, C.; Voliani, V.; Menichetti, L. Enhanced Photoacoustic Signal of Passion

Fruit-Like Nanoarchitectures in a Biological Environment. *J. Phys. Chem. C* **2017**, *121*, 6955–6961.
20. Armanetti, P.; Pocoví-Martínez, S.; Flori, A.; Avigo, C.; Cassano, D.; Menichetti, L.; Voliani, V. Dual photoacoustic/ultrasound multi-parametric imaging from passion fruit-like nano-architectures. *Nanomedicine Nanotechnology, Biol. Med.* **2018**, *14*, 1787–1795.
21. Vlamidis, Y.; Voliani, V. Bringing Again Noble Metal Nanoparticles to the Forefront of Cancer Therapy. *Front. Bioeng. Biotechnol.* **2018**, *6*.
22. Cassano, D.; Rota Martir, D.; Signore, G.; Piazza, V.; Voliani, V. Biodegradable hollow silica nanospheres containing gold nanoparticle arrays. *Chem. Commun.* **2015**, *51*, 9939–9941.
23. Cassano, D.; Summa, M.; Pocoví-Martínez, S.; Mapanao, A.-K.; Catelani, T.; Bertorelli, R.; Voliani, V. Biodegradable Ultrasmall-in-Nano Gold Architectures: Mid-Period In Vivo Distribution and Excretion Assessment. *Part. Part. Syst. Charact.* **2019**, *36*, 1800464.
24. Cassano, D.; Mapanao, A.K.; Summa, M.; Vlamidis, Y.; Giannone, G.; Santi, M.; Guzzolino, E.; Pitto, L.; Poliseno, L.; Bertorelli, R.; et al. Biosafety and biokinetics of noble metals: the impact of their chemical nature. *ACS Appl. Bio Mater.* **2019**, acsabm.9b00630.
25. Pocoví-Martínez, S.; Cassano, D.; Voliani, V. Naked Nanoparticles in Silica Nanocapsules: A Versatile Family of Nanorattle Catalysts. *ACS Appl. Nano Mater.* **2018**, *1*, 1836–1840.
26. d'Amora, M.; Cassano, D.; Pocoví-Martínez, S.; Giordani, S.; Voliani, V. Biodistribution and biocompatibility of passion fruit-like nano-architectures in zebrafish. *Nanotoxicology* **2018**, 1–9.
27. Langhans, S.A. Three-dimensional in vitro cell culture models in drug discovery and drug repositioning. *Front. Pharmacol.* **2018**, *9*, 1–14.
28. Verjans, E.-T.; Doijen, J.; Luyten, W.; Landuyt, B.; Schoofs, L. Three-dimensional cell culture models for anticancer drug screening: Worth the effort? *J. Cell. Physiol.* **2018**, *233*, 2993–3003.
29. Xin, X.; Yang, H.; Zhang, F.; Yang, S.T. 3D cell coculture tumor model: A promising approach for future cancer drug discovery. *Process Biochem.* 2019, *78*, 148–160.
30. Cole, R.W. Matrigel® as 3D culture medium: 2D vs. 3D changes in proliferation and ultrastructure. *Biomed. J. Sci. Tech. Res.* **2017**, *1*.
31. Rovithi, M.; Avan, A.; Funel, N.; Leon, L.G.; Gomez, V.E.; Wurdinger, T.; Griffioen, A.W.; Verheul, H.M.W.; Giovannetti, E. Development of bioluminescent chick chorioallantoic membrane (CAM) models for primary pancreatic cancer cells: A platform for drug testing. *Sci. Rep.* **2017**, *7*, 1–13.
32. Mapanao, A.K.; Voliani, V. Three-dimensional tumor models: Promoting breakthroughs in nanotheranostics translational research. *Appl. Mater. Today* **2020**, *19*, 100552.
33. Mapanao, A.K.; Voliani, V. Three-dimensional tumor models: Promoting breakthroughs in nanotheranostics translational research. *Appl. Mater. Today* **2020**, *19*, 100552.
34. Lu, H.; Stenzel, M.H. Multicellular Tumor Spheroids (MCTS) as a 3D In Vitro Evaluation Tool of Nanoparticles. *Small* **2018**, *14*, 1702858.
35. Mapanao, A.K.; Santi, M.; Faraci, P.; Cappello, V.; Cassano, D.; Voliani, V. Endogenously Triggerable Ultrasmall-in-Nano Architectures: Targeting Assessment on 3D Pancreatic Carcinoma Spheroids. *ACS Omega* **2018**, *3*, 11796–11801.
36. Busch, C.-J.; Becker, B.; Kriegs, M.; Gatzemeier, F.; Krüger, K.; Möckelmann, N.; Fritz, G.; Petersen, C.; Knecht, R.; Rothkamm, K.; et al. Similar cisplatin sensitivity of HPV-positive and -negative HNSCC cell lines. *Oncotarget* **2016**, *7*, 35832–35842.
37. European Parliament Directive 2010/63/EU - On the protection of animals used for scientific purposes.
38. Foty, R. A Simple Hanging Drop Cell Culture Protocol for Generation of 3D Spheroids. *J. Vis. Exp.* **2011**, *20*, 4–7.
39. Hall, M.D.; Dillon, C.T.; Zhang, M.; Beale, P.; Cai, Z.; Lai, B.; Stampfl, A.P.J.; Hambley, T.W. The cellular distribution and oxidation state of platinum(II) and platinum(IV) antitumour complexes in cancer cells. *JBIC J. Biol. Inorg. Chem.* **2003**, *8*, 726–732.